



Cite this: *Environ. Sci.: Nano*, 2025,
12, 3623

Antibacterial efficacy of light-activated graphene oxide nanoparticles and nanochitosan in water†

Rahul Chetry,^a Adityasukumar Pasagadi,^{ab} Muhammad Zubair,^a Aman Ullah ^a and M. S. Roopesh ^{a*}

Water quality is a crucial aspect of public health, and microbial contamination remains a significant challenge, necessitating the exploration of innovative water treatment methods. This study investigated the inactivation of *Escherichia coli* AW 1.7 in water driven by light-emitting diodes (LEDs) emitting UV-A (365 nm), near UV-visible (395 nm), and blue (455 nm) light in combination with graphene oxide (GO) nanoparticles (NPs) and nanochitosan (NC). The *E. coli* inoculum was added to NP suspensions (0.2 and 0.3% of GO and NC) and treated with the LED for 10 and 20 min. Results demonstrated that all GO treatments with different LED units reduced *E. coli* populations below the limit of detection (LOD) ($>5 \log \text{CFU mL}^{-1}$). In the case of NC (0.2 and 0.3%), UV-A was more effective on the photocatalytic inactivation with $>5 \log \text{CFU mL}^{-1}$ reduction in the *E. coli* population. The combination of NPs, H_2O_2 , and the 365 nm LED also gave significant (p -value < 0.05) *E. coli* reductions. Among individual LED treatments, UV-A was more effective in inactivating *E. coli*. The higher oxidation-reduction potential (ORP), electrical conductivity, and lower pH contributed to the greater *E. coli* inactivation with GO and LED combination treatments. The Fourier-transform infrared spectroscopy showed partial photoreduction of oxygen-containing functional groups in GO, while the structure of NC remained relatively unchanged. The study suggests the photocatalytic antibacterial potential of GO and NC, highlighting their application in water treatment.

Received 24th February 2025,
Accepted 6th May 2025

DOI: 10.1039/d5en00210a

rsc.li/es-nano

Environmental significance

Waterborne diseases remain a global challenge, with microbial contamination posing significant risks to public health and environmental sustainability. This study addresses the need for advanced, eco-friendly water treatment methods by demonstrating the photocatalytic antibacterial efficacy of graphene oxide (GO) nanoparticles and nanochitosan (NC) under UV-LED irradiation. The research highlights the synergistic interaction of nanomaterials and light in achieving effective microbial inactivation while minimizing harmful by-products. These findings can be generalized to broader applications in water treatment systems, particularly in resource-constrained settings. The work underscores the environmental significance of integrating nanotechnology and LED-based disinfection processes to develop safe, potentially energy-efficient, and sustainable solutions for global water quality management.

1. Introduction

Access to safe and readily available water is a fundamental human right. However, over 2.2 billion people lack access to clean water sources,¹ contributing to water-related diseases with over 3.4 million deaths each year, predominantly among children.² Diarrhea, often resulting from untreated, contaminated water, accounts for approximately 1 million of these deaths annually.¹ With a commitment to providing universal access to safe water by 2030, addressing water-related issues is crucial. Microbial contamination of water

poses a significant threat to various industries, especially the food processing industry, where the quality and safety of water are essential.^{3,4} The demand for clean water underlines the necessity for effective water treatment systems.⁵

A combination of primary, secondary, and tertiary water treatment methods are used, and each of these methods plays a vital role in achieving clean water. They eliminate different concentrations of pollutants as the water moves through each stage and are well-known for their effective sterilization and lasting impact on a broad spectrum of waterborne pathogens, including bacteria and viruses.^{6,7} Despite their effectiveness against bacteria, some of these chemical disinfectants, such as chlorine, can produce disinfection by-products in water, which are associated with increased risks to human health, including bladder cancer and negative reproductive effects.^{8–10} Moreover, current disinfection methods face significant challenges, including the substantial expenses associated with

^a Department of Agricultural, Food and Nutritional Science, University of Alberta, Edmonton, Alberta T6G 2P5, Canada. E-mail: roopeshms@ualberta.ca

^b Dairy Engineering Section, ICAR-National Dairy Research Institute, Southern Regional Station, Bengaluru, Karnataka, India-560030

† Electronic supplementary information (ESI) available. See DOI: <https://doi.org/10.1039/d5en00210a>



equipment and chemical agents, as well as increasing resistance to antimicrobials.¹¹ The limitations of conventional disinfectants lead to seeking novel alternatives that can overcome these disadvantages.¹²

With the rapid advancement of the semiconductor industry, UV radiation can now be generated by UV light-emitting diodes (UV-LEDs), offering an effective and economically viable alternative to conventional UV lamps.^{13,14} UV-LEDs are compact devices that produce mercury-free light.^{15,16} They offer an effective solution for inactivating a wide range of pathogenic microorganisms in water.¹⁷ Additionally, they are cost-effective, and have a long operational lifetime, making them suitable for integrating into existing processing lines without producing toxic disinfection by-products.^{10,18} The light pulses emitted by LEDs at wavelengths of 365 nm (UV-A), 395 nm (near UV-visible; NUV-Vis), and blue light (455 nm) demonstrated promising antibacterial effects in food systems.¹⁹

The integration of nanotechnology to develop new treatment methods is a promising alternative to conventional disinfection methods. They exhibit excellent adsorption and catalytic behaviour owing to their large specific surface area and high reactivity.²⁰ Recently, various natural and engineered nanomaterials have exhibited potent antimicrobial properties, the most researched among them are silver NPs, zinc oxide (ZnO) and copper oxide NPs.²¹ In addition to all these engineered NPs, NC and GO have drawn significant interest owing to their unique properties and mode of bacterial inactivation.²² NC, prepared from a biopolymer, chitosan, exhibits high antimicrobial activity, and it possesses a positive charge that allows it to interact with negatively charged microbial cell membranes, rupturing them and allowing leakage of cellular components.²³ In contrast to this, GO offers a high surface area with strong oxidative potential capable of damaging bacterial cell membranes through the induction of oxidative stress *via* ROS generation.²⁴ The combination of these NPs, such as NC and GO, with light pulse emitting LEDs (365, 395, and 455 nm) is likely to enhance the antibacterial properties synergistically by amplifying the oxidative stress on the microbial cells *via* enhanced reactive oxygen species (ROS) production, leading to cellular damage.

In recent times, advanced oxidation processes (AOPs) have gained significant importance in wastewater treatment.²⁵ AOPs comprise of UV treatment in combination with secondary oxidants, such as H₂O₂, O₃, or PAA, which can generate ·OH of highly reactive nature through photocatalytic degradation.²⁶ These ·OH radicals are very effective in degrading a wide range of organic contaminants, decreasing the formation of disinfection by-products, and effectively inactivating microorganisms, making them a versatile tool for water treatment.²⁶ Despite these advancements, there still exists a research gap in understanding the combined effect of AOPs and NPs on bacterial inactivation. We anticipate that the introduction of H₂O₂ to NC or GO NP suspensions followed by UV-LED irradiation could enhance oxidative

stress by increasing the generation of ROS, leading to cell death. This study investigated the inactivation of heat and oxidizer (*e.g.*, chlorine, hydrogen peroxide) resistant *E. coli* AW 1.7 in water using a combination of NPs, LEDs, and H₂O₂ individually and in different combinations with varying NP and H₂O₂ concentrations and LED treatment times. *E. coli* was selected for this study because it is the most common indicator for identifying fecal contamination in drinking water supplies globally.

2. Materials and Methods

2.1. Bacterial culture preparation

E. coli AW 1.7 was used as the model microorganism to assess its inactivation during light-activated NP treatment. The bacterial isolate was first restored from frozen stock by streaking on tryptic soy agar plates (TSA; Becton, Dickinson and Company, Franklin Lakes, NJ, USA) supplemented with 0.6% (w/v) yeast extract (YE; Fischer Bioreagents, Geel, Belgium) and incubated for 24 h at 37 °C (Fig. 1A). This process was followed by two consecutive transfers into 5 mL of sterile tryptic soy broth (TSB; Becton, Dickinson and Company, Franklin Lakes, NJ, USA) supplemented with 0.6% YE, with incubation periods of 24 h and 20 h at 37 °C, respectively.

Subsequently, 100 µL of the *E. coli* culture was spread onto tryptic soy agar with 0.6% yeast extract (TSAYE) plates and incubated for 24 h at 37 °C. The resulting bacterial lawn was harvested with 2 mL of 0.1% (w/v) peptone water (Fischer Bioreagents, Geel, Belgium) and collected into a 1.5 mL Eppendorf tube. This was followed by centrifugation at 10 000 × g for 5 min and further removal of the supernatant, the pellet was suspended again with peptone water to make up to 1 mL of total volume.

2.2. NP suspension preparation and inoculation

In this study, two different types of NPs were investigated, including NC (20–150 nm in size) and GO (100–400 nm in size). The preparation methods and detailed structural characterization of the nanoparticles are provided in the ESI† files. Three NP suspensions were prepared: 0.1%, 0.2%, and 0.3%. Each concentration was achieved by mixing 0.1, 0.2, and 0.3 g of the respective NP in 100 mL of distilled water. The mixtures were homogenized using a magnetic stirrer at ambient temperature for 24 h before subsequent treatment (Fig. 1B).

The *E. coli* culture (0.1 mL) was added to 100 mL of 0.1% NC and GO suspensions under sterile conditions overnight. Based on the experimental design, the inoculated suspensions were mixed using a magnetic stirrer for 1 h. This procedure was designed to investigate the antibacterial efficacy of the NP and to determine whether a 1 h waiting time could result in significant bacterial reduction. Similarly, the control was prepared by inoculating 0.1 mL of the bacterial culture with 100 mL of distilled water while holding it for 1 h using a magnetic stirrer. The resultant mixtures were plated and enumerated on TSAYE plates.



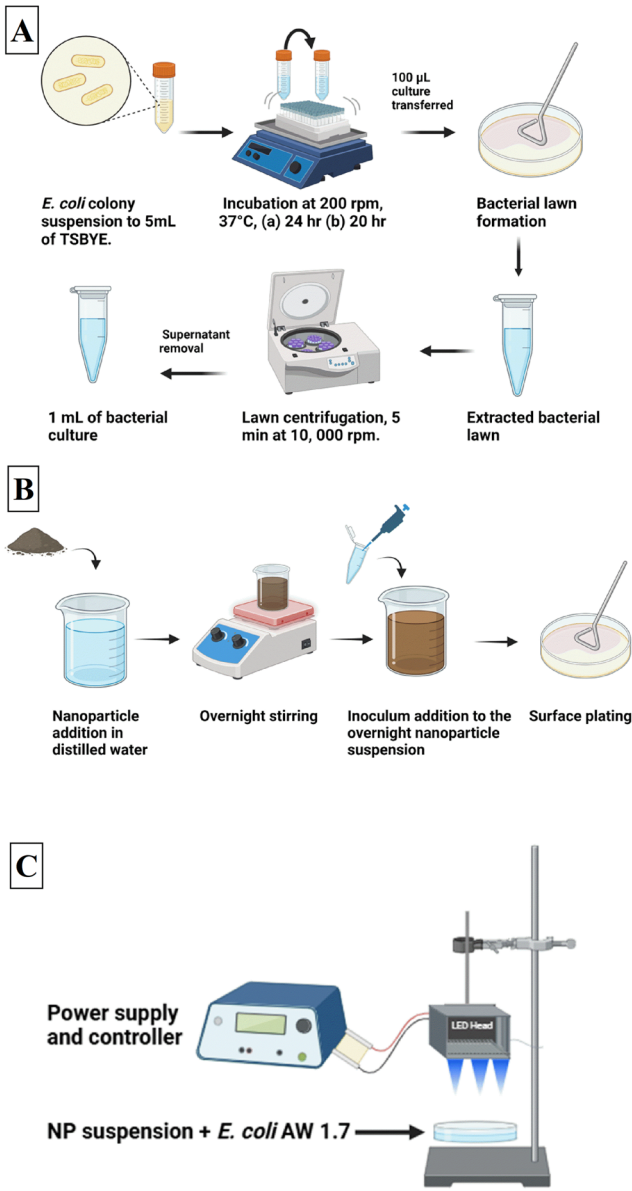


Fig. 1 *E. coli* treatment in NP suspension, preparatory stages: (A) bacterial culture preparation; (B) NP suspension preparation; (C) LED treatment set-up.

2.3. Light emitting diode (LED) system

The LED system comprised of a bench-top controller (CF3000, Clearstone Technologies Inc., Hopkins, MN, USA) compatible with the JL3 series LED heads (11.1 cm × 7 cm × 12.8 cm). The unit emits light of different wavelengths, including ultraviolet-A (UV-A, 365 nm), near UV-visible (NUV-Vis, 395 nm), and blue (455 nm) light. The UV-LEDs were positioned facing downward, placed 2 cm above the surface of a 10 mL sample contained in a sterile Petri dish (60 × 15 mm), and treated for 10 and 20 min, respectively. The irradiance of the 365, 395, and 455 nm LEDs was measured using a laser energy meter (7Z01580, Starbright, Ophir Photonics, a Newport Company, Har Hotzvim, JRS, Israel), which was connected to a photodiode irradiance and dose

sensor (PD300RM-8 W, Ophir Photonics, A Newport Corporation Brand, Har Hotzvim, JRS, Israel). The corresponding dose for 365, 395, and 455 nm LEDs treated for 10 and 20 min was calculated as the product of the LED light's irradiance (W cm^{-2}) and the exposure duration, in seconds (s) (ESI† data S1).²⁷ A power level of 60% was employed, corresponding to 'ON' and 'OFF' times of 6 ms and 4 ms, respectively. The various treatment parameters, such as height, power level, and treatment time, were determined based on preliminary experiments.

2.4. UV-LED + NP treatment on *E. coli* inactivation

NP suspensions at concentrations of 0.2% and 0.3% were prepared by mixing 20 mg and 30 mg of NC and GO in 10 mL of distilled water (DW), respectively. The suspensions were prepared in small Petri plates, sealed with parafilm, and stirred for 24 h under sterile conditions. The suspension mixtures were inoculated with 10 μL of *E. coli* culture, which accounts for 0.1% in 10 mL of distilled water. Post-inoculation, the suspensions were vortexed for 2 min to ensure uniformity. The NP suspensions were then exposed to light pulses with wavelengths of 365 nm, 395 nm, and 455 nm, emitted from the LED at an LED power level set to 60% and a height of 2 cm from the samples (Fig. 1C). The LED treatments were conducted for 10 and 20 min for the samples with 0.2% NP concentration, while the samples with 0.3% NP concentration were treated only for 10 min.

The *E. coli* suspension samples treated with LEDs alone without NPs were considered the positive control. Further, the second set of positive control samples included *E. coli* suspension samples without NPs. The treated and untreated samples were serially diluted in sterile 0.1% (w/v) Peptone Water (Fischer Bioreagents, Geel, Belgium) and viable cell counts were obtained by surface plating on TSAYE plates, followed by incubation for 20–24 h at 37 °C. Results were expressed as log CFU mL^{-1} , and the LOD was determined.

2.5. Combined effect of H_2O_2 , NPs, and UV LED treatment on *E. coli* inactivation

Twenty mg of NC and GO were dissolved in 10 mL of DW overnight to produce NP suspensions with a concentration of 0.2%. The mixture was placed in a small Petri plate, sealed with parafilm, and stirred continuously for 24 h under sterile conditions. The NC and GO NP suspensions were inoculated with 10 μL of *E. coli* culture and subsequently vortexed for 2 min to ensure uniformity. H_2O_2 was added at concentrations of 0.1 and 0.01 M by mixing 102 μL and 10.2 μL of H_2O_2 , respectively, into 10 mL of the prepared suspension. The mixtures were vortexed for an additional 5 s. The NP suspensions were then exposed to 365 nm light pulses emitted from the LED for 1 and 3 min (Fig. 1C). Specifically, the NP suspensions with 0.1 M were treated for 1 min, and the NP suspensions with 0.01 M H_2O_2 concentration were treated for 1 and 3 min. Positive and negative control samples (treatments only with NPs, H_2O_2 , LEDs, and those without any treatments)

were used to compare the combined effect of $\text{H}_2\text{O}_2 + \text{NP} + \text{LED}$ on inactivation efficacy. For the control samples, a waiting time corresponding to the LED exposure time was implemented. The treated samples without LEDs were held for the same duration as the LED treatment time before subsequent plating. The treated and untreated samples were serially diluted in sterile TSBYE and viable cell counts were obtained by spread plating on TSAYE plates, followed by incubation at 37 °C for 20–24 h. Results were expressed as log CFU mL^{-1} , and the LOD was determined.

2.6. Determination of the ORP, pH, and electrical conductivity of the treated water samples

The ORP, pH, and the electrical conductivity of the samples without *E. coli* inoculation were determined using an ORP meter (ITM Instruments, Canada), a pH meter (ITM Instruments, Canada), an electrical conductivity meter (Fisher Scientific, Canada), and a digital thermometer (Gain Express Holdings Ltd., HK). In the case of NP + LED treatment, NC and GO NP suspensions were prepared following the same procedure for the *E. coli* inactivation experiments. These suspensions were then exposed to light pulses emitted from the LED at wavelengths of 365 nm, 395 nm, and 455 nm, respectively. The ORP, pH, and electrical conductivity of the treated samples were measured within 2 min of the treatment. Control samples, including NP and LED treatment alone, were also evaluated. In the case of NP + $\text{H}_2\text{O}_2 + \text{LED}$ combined treatment, NC and GO NP suspensions at a concentration of 0.2% were mixed with 0.1 M and 0.01 M H_2O_2 . The suspensions were vortexed for 5 s and then exposed to light pulses with 365 nm emitted from the LED. The treatment times were 1 and 3 min, with the 0.1 M H_2O_2 suspension only treated for 1 min. The ORP, pH, and electrical conductivity of the treated samples were determined and compared to control samples. Positive control samples included water samples treated with H_2O_2 alone, UV alone, NP alone, $\text{H}_2\text{O}_2 + \text{UV}$, $\text{H}_2\text{O}_2 + \text{NP}$, and NP + UV without *E. coli*.

2.7. Scanning electron micrograph (SEM) analysis

The morphological characteristics of the NP (NC and GO) were examined using the ZEISS EVO 10 SEM (Munich, Germany). The NP was analyzed without any prior treatments. The images provided detailed information on the size, shape, and surface features of the NP, allowing for a comprehensive analysis of their morphological properties.

2.8. Fourier transform infrared (FTIR) spectroscopy

FTIR spectroscopy was used to analyse the functional groups of the LED-treated NP. NC and GO samples treated with LEDs (365, 395, and 455 nm) were prepared for FTIR analysis. A 0.2% overnight suspension of each NP was prepared by mixing 20 mg of each NP with 10 mL of DW and exposed to the light sources for 20 min. Dry-NC/GO represents the untreated powder NP, and Wo/T-NC/GO represents the dried

NP extracted from 10 mL of aqueous suspension without LED treatment. The treated liquid samples were dried using a rotatory evaporator (PE-8910, Europe). The spectra were recorded using an attenuated total reflectance-FTIR Nicolet 8700 spectrometer (Madison, WI, USA) over a wavenumber range of 4000 to 400 cm^{-1} .

2.9. Statistical analysis

All bacterial inactivation experiments were performed three independent times ($n = 3$), whereas data on the concentration of ORP, pH, and electrical conductivity were obtained from two replicates ($n = 2$). Values from all experiments were expressed as the mean \pm standard deviation (SD). Statistical analysis was performed using the Origin Pro (2023b) statistical tool. One and two-way analyses of variance (ANOVA) were conducted to compare the effects of different treatment conditions on the bacterial reduction and concentration of ORP, pH, and electrical conductivity. The significant differences between mean values were identified by Tukey's test with a confidence level of $P \leq 0.05$.

3. Results and discussion

3.1. Antibacterial properties of NC and GO NPs

While investigating the antibacterial effectiveness of the different NP suspensions in this study, GO was found to be highly effective against *E. coli* in water (Fig. 2). For instance, the GO NP demonstrated a strong concentration-dependent effect for 0.2 and 0.3% GO compared to 0.1% GO with significant ($P < 0.05$) reductions in *E. coli* inactivation population of 2.35 and 2.02 log CFU mL^{-1} , respectively. The greater inactivation efficacy of GO could be partly attributed to its toxicity mechanism, which induces oxidative stress by the generated ROS, similar to other carbon-based and other

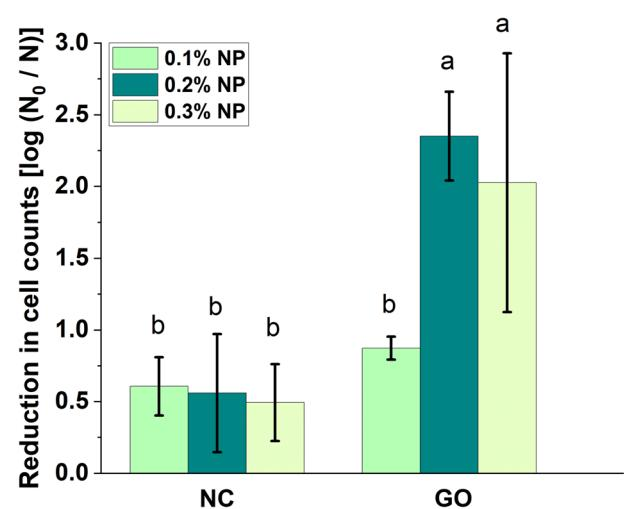


Fig. 2 The *E. coli* inactivation efficacy of NPs (NC and GO) at 0.1, 0.2, and 0.3% concentrations. Results are shown as mean \pm standard deviation of triplicate independent experiments. Here, N_0 represents the CFU mL^{-1} in control samples and N represents the CFU mL^{-1} in the treated samples. Error bars indicate the standard deviation ($n = 3$).



nanoscale materials. For example, O_2^- anions are produced by graphene-based materials.²⁸ This can facilitate the production of other ROS, such as 1O_2 and $^{\bullet}OH$ radicals, contributing to the antibacterial activity of GO.^{28,29} However, more studies are needed to confirm this argument. The antimicrobial activity of GO can also be attributed to oxygen-containing surface functional groups of GO (*i.e.*, epoxides, hydroxyls, carboxyls). The surface functional groups can interact with cell membranes, inducing oxidative stress, membrane damage, and intracellular ROS accumulation. The basal ROS generation in this context is typically a result of redox reactions at the GO-bacteria interface.³⁰

A previous study has reported the ROS-independent oxidative stress mediated by graphene-based materials as well, where they disrupt or oxidize a specific cellular component without ROS generation.²⁹ This mechanism was previously validated by examining the % loss of glutathione (GSH), an essential antioxidant in bacterial cells.³¹ The loss of GSH was reported to be highly reliant on GO's concentration, suggesting that increased concentrations of GO enhance oxidative stress through the depletion of GSH.²⁴ This concept partially supports our finding, where we observed a clear correlation between the level of *E. coli* inactivation and the concentration of GO used. Additionally, the higher level of *E. coli* inactivation could be accompanied by certain morphological changes, where the *E. coli* cell becomes flattened and eventually loses its cellular integrity, resulting in irreversible damage in the GO suspension.⁵

In this study, the *E. coli* reductions were minimal across 0.1, 0.2, and 0.3% NC concentrations, with a maximum of 0.6 log reductions at 0.1% NC concentration. (Fig. 2). NC interacts with the negatively charged bacterial surface due to its higher surface charge density, leading to an electrostatic interaction.³² This disrupts the cells, resulting in the loss of essential cellular components, ultimately leading to the death of the *E. coli* cells.³² However, the *E. coli* inactivation in the case of NC was significantly lower ($p < 0.05$) than GO NP suspensions. This could likely be due to the possible aggregation with NC in water, particularly at an increased concentration. These aggregations at higher NC concentrations could form a layer around the bacterial cell, but not necessarily attached to the bacterial surface, lowering the inactivation effectiveness. This aligns well with a previous study reported by Goy and coworkers.³³ Conversely, the lower inactivation observed with NC compared to GO could be due to GO's higher surface area and oxidative stress-inducing properties, which enhance its antimicrobial activity.

3.2. Antibacterial efficacy of 365, 395, and 455 nm LED treatments

The results indicated that the 365 nm LED treatment was more effective (Fig. 3). The 10 min of 365 nm LED treatment led to a substantial reduction in the *E. coli* population. For instance, *E. coli* reductions of ~ 2.6 log CFU mL^{-1} in water were observed after a 365 nm LED treatment

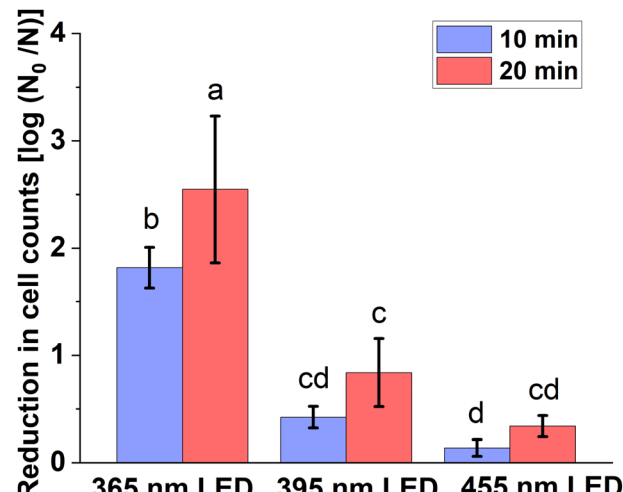


Fig. 3 The *E. coli* inactivation efficacy of LED treatments (365 nm, 395 nm, and 455 nm) for 10 and 20 min. Results are shown as mean \pm standard deviation of triplicate independent experiments. Here, N_0 represents the CFU mL^{-1} in the control and N represents the CFU mL^{-1} in the treated samples. Error bars indicate the standard deviation ($n = 3$).

time of 20 min (Fig. 3). The greater bacterial inactivation of the 365 nm LED has been previously reported in the literature.^{19,34,35} The greater efficiency of the 365 nm LED, which lies within the near-UV spectrum, can be attributed to its ability to generate ROS and induce oxidative deoxyribonucleic acid (DNA) damage, as highlighted in a previous study.³⁴ Specifically, the 365 nm LED produces greater quantities of 8-hydroxy-2'-deoxyguanosine (8-OHdG), a crucial biomarker of DNA oxidative damage.³⁶

The 365 nm UV-A LED emits light in the near-UV range, with photon energy high enough to excite molecular bonds and trigger the production of reactive oxygen species (ROS) *via* multiple mechanisms. Firstly, UV-A exposure can directly photolyze dissolved water and oxygen, leading to the formation of hydroxyl radicals ($^{\bullet}OH$) and superoxide anions (O_2^-).³⁷ Secondly, bacterial cells contain endogenous chromophores—such as porphyrins and flavins—that absorb UV-A light and undergo photodynamic activation, thereby increasing intracellular ROS levels, oxidative stress, and causing membrane damage.³⁸

On the other hand, the 395 nm LED resulted in significantly lower ($P < 0.05$) *E. coli* reductions than the 365 nm LED (Fig. 3). The 395 nm LED requires a relatively higher dosage to produce the same level of microbial inactivation compared to the 365 nm LED. It could be anticipated that the 395 nm LED cannot emit enough UV-A light to inactivate bacteria in the water. Additionally, the 395 nm LED treatment at higher treatment time was not significantly ($P < 0.05$) more effective than the 455 nm LED treatment, except for the 10 min 395 nm LED treatment, which showed a significant difference ($P < 0.05$). The greater wavelength LED is far less effective at inducing DNA damage compared to other 365 nm LED treatments despite displaying higher dose values of



386.7 J cm⁻² (ESI† Table S1). In previous studies,^{39–41} it was observed that the 405 nm LED treatment did not significantly induce DNA oxidation, although it showed bacterial membrane disruption. This underscores the importance of wavelength selection in LED-based disinfection systems, as the wavelength used was found to be more important than the dose in effectively inactivating *E. coli*.

3.3. Effects of combined (NP + LED) treatments on the inactivation of *E. coli*

3.3.1. Antibacterial efficacy of light-activated GO NPs. Results demonstrated that all the LED treatments (365, 395, and 455 nm) for 10 and 20 min with both GO concentrations (0.2% and 0.3%) resulted in the inactivation of *E. coli* below the LOD (>5 log CFU mL⁻¹ reduction) (Fig. 4). The GO NP was highly effective in the inactivation of *E. coli* across all tested LED concentrations and treatment times, showcasing its highly photocatalytic antimicrobial nature. As described in the above sections, the individual LED and GO treatments had limited efficacy in reducing the microbial population (Fig. 2 and 3). The light-activated GO significantly increased

the level of microbial inactivation, indicating a synergistic interaction between GO and all the LED treatments used.

The level of effectiveness of light-activated GO can be explained by the activation of GO by light, leading to the production of ROS, particularly $^1\text{O}_2$, as reported in a previous study.²⁹ Additionally, we anticipate that the oxidation of glutathione (GSH) by light-activated GO suspension would be significantly enhanced upon exposure to LED treatments at different wavelengths. In a previous study, a significant increase in the level of GSH oxidation was observed upon exposure to simulated sunlight;²⁹ however, simulated sunlight is different from the LED wavelengths used in this study. In some earlier studies, these effects were found to increase as a function of LED treatment time.²⁹ This assumption, however, can be disregarded in our case since the bacterial inactivation levels were constant when GO and LED treatments were combined, regardless of the LED treatment duration. In contrast, recent studies indicate that GO's light-enhanced oxidation capability may not be primarily due to the oxidative stress introduced by the ROS. GO contains both sp^2 -hybridized (π -rich) and sp^3 -hybridized (σ -rich) domains due to surface oxidation. GO possesses

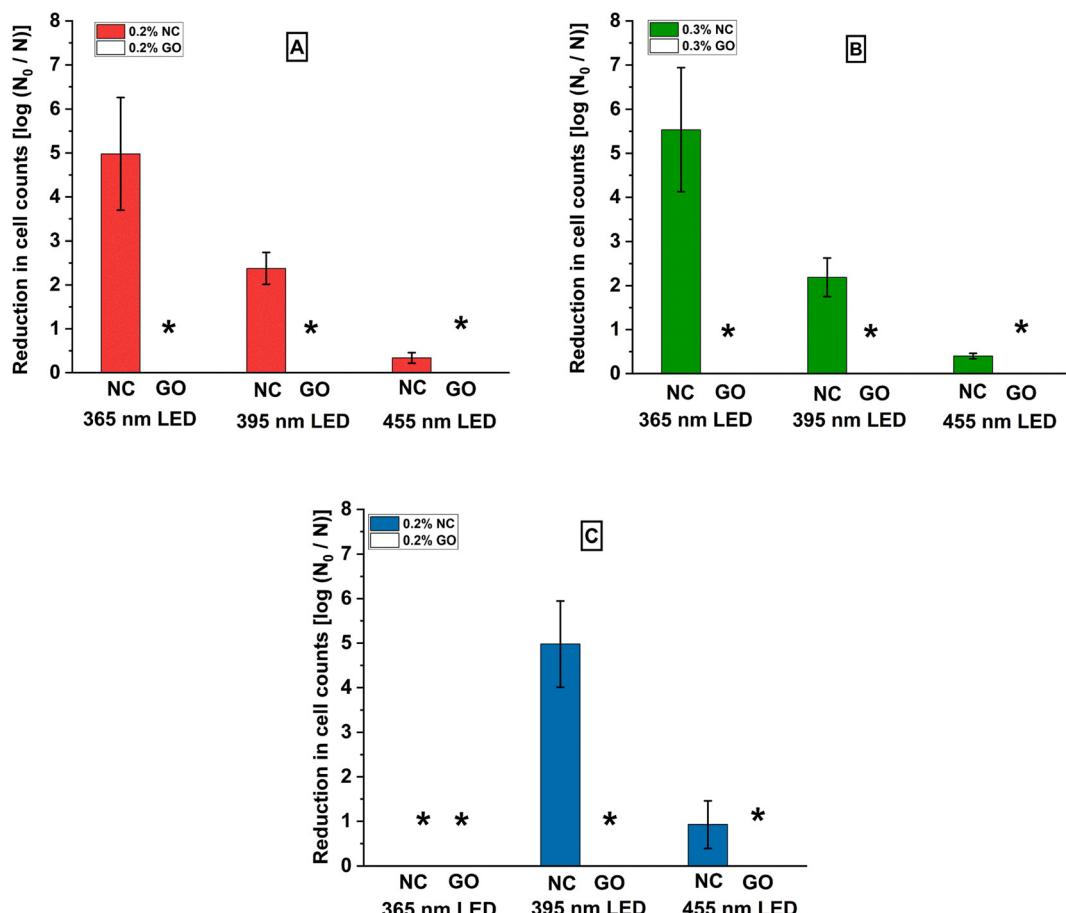


Fig. 4 The *E. coli* inactivation efficacy of 365, 395, and 455 nm LED + NP (NC and GO) (A) 0.2% NP concentration + 10 min LED treatment, (B) 0.3% NP concentration + 10 min LED treatment, (C) 0.2% NP concentration + 20 min LED treatment. Results are shown as mean \pm standard deviation of triplicate independent experiments. Here, N_0 represents the CFU mL⁻¹ in the control and N represents the CFU mL⁻¹ in the treated samples. Error bars indicate the standard deviation ($n = 3$). An asterisk (*) indicates the reduction of cell counts below the detection limit.



more significant energy gaps between the π -state from its sp^2 carbon sites and the σ -state of its sp^3 -bonded carbons.⁴² The disrupted electronic structure and presence of localized states enable GO to oxidize biomolecules such as GSH through direct electron transfer mechanisms, possibly independent of reactive oxygen species like singlet oxygen (1O_2). When GO interacts with GSH, it accepts electrons directly from electron-rich moieties such as thiol groups, resulting in their oxidation.³⁰

The oxygen functional groups, such as hydroxyl ($-OH$), carboxyl ($-COOH$), and epoxy ($-C-O-C$) groups at the basal plane and the edges of the GO, are slightly activated upon light treatment.⁴³ It has been reported that prolonging the UV treatment time could result in the reduction of GO.⁴⁴ When GO is exposed to light, the oxygenated functional groups, such as hydroxyl, epoxy, and carboxyl, which are present on the base and edges of the graphene oxide, generate ROS. For instance, electrons could be excited from the valence to the conduction band by UV-A light and create electron-hole pairs.⁴⁵ These photo-excited electrons could reduce O_2 to produce superoxide radicals (O_2^-), while the holes can oxidize water molecules to produce hydroxyl radicals ($^{\cdot}OH$). These reactive species have the potential to harm cellular structures. In addition, the reduction of GO removes many of these oxygen groups, restoring conjugated domains and changing its reactivity. Reduced graphene oxide is more toxic as it aggregates more due to reduced hydrophilicity and increased $\pi-\pi$ stacking.⁴⁶ These compact aggregates increase ROS generation in adherent cells, thereby showing enhanced toxicity.⁴⁷

The inactivation of bacterial cells at all the LED wavelengths (365 nm, 395 nm, and 455 nm) in combination with GO shows that GO possesses high photocatalytic antimicrobial activity at different excitation energies. The 365 nm LED (UV-A) may have a higher photon energy, which can excite GO more than the 395 nm and 455 nm LEDs; however, their photon energies may be sufficient to cause microbial inactivation when GO is present. Other studies have shown longer wavelengths to be less efficient in photocatalytic activation by providing insufficient energy to overcome the bandgap or generate electron-hole pairs; our results show GO to remain efficient under these conditions.⁴⁸ This could be due to possible narrowing effects on the bandgap in GO, surface defects, or other light absorption mechanisms that facilitate visible light activation to some degree.⁴⁸ Significantly, control treatments with LEDs only (*i.e.*, without GO) produced minimal microbial reductions, particularly at 395 and 455 nm, confirming that GO is a major contributor to the antibacterial activities obtained at all three wavelengths.

These findings validate a synergistic interaction of GO with all of the LED treatments and emphasize the potential of GO as a broad-spectrum photocatalyst for antimicrobial applications in the near-UV and visible light range.³⁰

3.3.2. Antibacterial efficacy of light-activated NC. In the case of combined treatment with NC, the specific interaction between the NC and the type of LED used had a substantial impact on the degree of *E. coli* inactivation. Statistically, the

365 nm LED treatment was more effective on the photocatalytic inactivation of *E. coli* compared to the 395 nm and 455 nm LED at both tested concentrations, 0.2% and 0.3%, respectively (Fig. 4). In the case of combined treatment with NC, interaction with the 365 nm LED resulted in *E. coli* inactivation below the detection limit ($>5 \log CFU \text{ mL}^{-1}$), which was substantially greater than that observed with either treatment alone ($\sim 2 \log CFU \text{ mL}^{-1}$ for the 365 nm LED alone and $<0.6 \log$ for NC alone). This enhanced reduction is indicative of a synergistic photocatalytic inactivation mechanism, where 365 nm UV-A light excites endogenous bacterial chromophores such as porphyrins and flavins, leading to intracellular generation of reactive oxygen species (ROS), including singlet oxygen (1O_2) and hydroxyl radicals ($^{\cdot}OH$). NC complements this effect by disrupting membrane integrity through electrostatic interactions with the negatively charged bacterial envelope, thereby increasing permeability to oxidative stress. Additionally, the surface-active and flocculating properties of NC may facilitate localized ROS concentration at the bacterial surface, amplifying damage. Although NC does not function as a classical semiconductor photocatalyst, its role in promoting a light-amplified, ROS-mediated antimicrobial response aligns with the functional interpretation of photocatalytic inactivation in biological systems. The antibacterial effectiveness reduced with increasing LED wavelength for the light wavelengths tested in this study. These results align well with a previous study,⁴⁹ where the sensitivity of coproporphyrin to UV light was found to increase with shorter wavelengths, which could explain the enhanced photocatalytic inactivation of *E. coli* observed with the 365 nm LED treatment.

Primarily, the cationic molecules of chitosan can bind with the anionic phospholipids present in the bacterial cell membrane, thereby causing disintegration of the cell.⁵⁰ In addition, the ROS generated by intracellular porphyrins activated by LED treatments could oxidize the genetic components, such as DNA, along with the membrane protein. These mechanisms suggest that chitosan combined with LED treatments may simultaneously affect the bacterial membranes and internal structures, thus creating a synergistic antibacterial effect. Additionally, the NC + 365 nm LED treated samples had an *E. coli* reduction level either below or close to the detectable limit (Fig. 4). There was an increasing trend in the *E. coli* inactivation with the increase in LED treatment time from 10 to 20 min when combined with the NP, especially in the case of NC (Fig. 4A and C).

When comparing how each NP responded to an individual LED at a time, GO displayed significantly ($P < 0.05$) higher *E. coli* inactivation efficacy with log reductions below the LOD (as mentioned previously) when combined with the 365 nm LED treatment. On the other hand, with all the LED treatments, NC was less effective than GO at a lower treatment time and concentration. However, with an increase in the LED treatment time and concentration, NC and GO suspension under 365 nm LED treatments resulted in reductions below the LOD.



3.4. *E. coli* inactivation by the combined treatment of NPs, H_2O_2 , and the 365-nm LED

The combination of NC (0.2%) with 0.1 M H_2O_2 and 365 nm LED treatment for 1 min resulted in an overall reduction below the LOD (Fig. 5A). Further, NC (0.2%) with 0.01 M H_2O_2 and 365 nm LED treatment for 1 and 3 min was also

effective in reducing the *E. coli* population in the water significantly achieving 1.79 log reduction at 1 min and 4.68 log reduction at 3 min (Fig. 5B and C). As there is limited existing literature on this, we anticipate a series of mechanisms that could have possibly led to greater effectiveness. Firstly, both H_2O_2 and LED light produce ROS; NC can enhance this generation owing to its high surface area and cationic nature, which promotes the adsorption of H_2O_2 , increasing the local concentration of reactive species and eventually enhancing ROS generation. This contributes to the overall effectiveness of the combined NC + H_2O_2 + 365 nm LED treatment in *E. coli* inactivation. It is possible that NC either enhances the production of ROS or is more effective with bacterial cells under both H_2O_2 and UV-A light conditions, causing a higher antibacterial effect, which requires further research.

The combination treatment of GO (0.2%) with 0.01 M H_2O_2 and 365 nm LED treatment for 1 and 3 min resulted in a significant ($P < 0.05$) reduction in the *E. coli* population in water, achieving 1.27 and 1.96 CFU mL^{-1} log reductions. Additionally, the combination treatment of GO (0.2%), 0.1 M H_2O_2 and 365 nm LED treatment for 1 min resulted in a significant *E. coli* reduction of 2.58 CFU mL^{-1} (Fig. 5). The addition of H_2O_2 to the suspension lowered the effectiveness of *E. coli* reduction compared to the H_2O_2 + 365 nm LED treatment. This observation could be attributed to the antioxidant activity of GO, which scavenges $\cdot\text{OH}$ radicals that play a crucial role in *E. coli* reduction.⁵¹ GO's large surface area offers abundant active sites for radicals to interact, enhancing its efficacy in scavenging reactive species.

Despite the lower inactivation efficacy of the 365 nm LED and the H_2O_2 alone, a reduction close to LOD was attained when 0.1 M H_2O_2 was irradiated with a 365 nm LED for 1 min (Fig. 5A). Similar observations were reported in a previous study⁵² when a UV-C lamp was used together with 11 mg L^{-1} H_2O_2 for 5 min. A lower concentration of H_2O_2 , *i.e.*, 0.01 M H_2O_2 treatment in combination with 365 nm LED treatment for 1 and 3 min, also resulted in significant ($P < 0.05$) reductions in the *E. coli* population in water, respectively (Fig. 5B and C). The excellent antibacterial effectiveness of H_2O_2 may be associated with its strong oxidizing property, which targets various biomolecules within the bacterial cells, causing peroxidation and disruption of the cellular membrane.⁵³

In our study, we observed a positive correlation between the duration of LED treatment and the concentration of H_2O_2 used (Fig. 5). The bacterial inactivation efficacy improved with a higher H_2O_2 concentration (0.1 M) and a short LED treatment time of 1 min. On the other hand, the lower concentration of H_2O_2 was readily compensated to a great extent by increasing the LED treatment duration to 3 min to achieve *E. coli* inactivation.

The current approach using NC, GO, H_2O_2 , and 365 nm UV LED treatment achieves rapid bacterial inactivation, with similar or outperforming antimicrobial efficacies of several previously reported nanomaterial-based disinfection methods

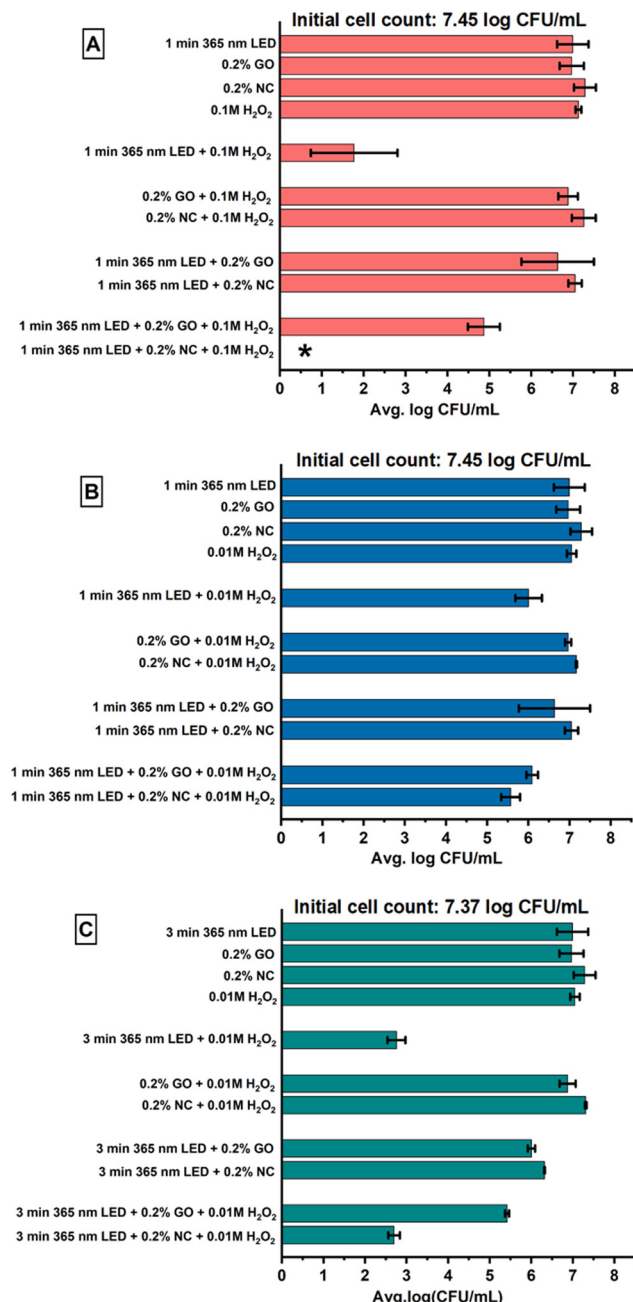


Fig. 5 The *E. coli* inactivation efficacy values of the combined treatments (365 nm + NP + H_2O_2): (A) 0.1 M H_2O_2 and 1 min LED treatment, (B) 0.01 M H_2O_2 and 1 min LED treatment and (C) 0.01 M H_2O_2 and 3 min LED treatment. Results are shown as mean \pm standard deviation of triplicate independent experiments. Here, N_0 represents the CFU mL^{-1} in control and N represents the CFU mL^{-1} in the treated samples. Error bars indicate the standard deviation ($n = 3$). An asterisk (*) indicates the reduction of cell counts below the detection limit.



Table 1 Comparative antibacterial efficacy of nanomaterial-based treatments for water disinfection

Nanoparticle	Treatment conditions	Antibacterial efficacy (log reduction)	Application and outcome
Chitosan nanoparticles (CS-NPs)	CS: 0.25%, 6 h	>4 log (99.99%) reduction in <i>E. coli</i> ATCC® 25922	Effective for water disinfection; strong antibacterial effect via membrane disruption ⁵⁴
Chitosan nanoparticles with UV-C irradiation	CS-NPs: 0.1%, UV-C 15 min	Below detection limit for <i>E. coli</i> O157:H7 and <i>L. monocytogenes</i>	Tested in pomegranate juice; UV enhanced chitosan nanoparticle activity for faster bacterial inactivation ⁵⁵
Graphene-TiO ₂ nanocomposite	TiO ₂ : 0.1%: graphene 0.25 mg mL ⁻¹ , 24 h incubation	3.04 log reduction in <i>E. coli</i> , 1.40 log reduction in <i>S. aureus</i>	Successfully tested for industrial wastewater treatment; inactivation via adsorption & ROS generation ⁵⁶
Silver nanoparticles (AgNPs)	AgNPs: 10 µg mL ⁻¹ exposure	Below detection limit for <i>E. coli</i> ATCC 8739	Antibacterial coatings and water disinfection; very effective but can cause nanoparticle aggregation in water ⁵⁷
Gold & silver nanoparticles (AuNPs & AgNPs)	AuNPs: 2 µg mL ⁻¹ (citrate), 5 µg mL ⁻¹ (PAH) AgNPs: 20 µg mL ⁻¹	AuNPs: 4 log reduction AgNPs: complete inhibition (~6 log reduction) in <i>E. coli</i>	Biomedical and antimicrobial coatings; AuNPs are effective but their high-cost limits large-scale application; AgNPs displayed strong antibacterial activity, but with aggregation issues ⁵⁸

(Table 1). However, caution should be warranted as an absolute comparison of the antimicrobial efficacies of NC, GO, H₂O₂, and 365 nm UV LED treatment (and their combinations) with previously reported water treatment methods is not possible as previous studies used different testing conditions, treatments, and specific species of bacteria with varying resistances to antimicrobial treatments. For instance, the current study reported a complete reduction of *E. coli* below the detection limit in short treatment times, whereas other nanomaterial-based approaches (Table 1) required longer treatment times and/or higher concentrations to achieve comparable effects. For instance, chitosan nanoparticles alone (CS-NPs) required 6 hours to achieve a 4-log reduction, whereas the current study reported a greater bacterial inactivation in just 1–3 min. The treatment using CS-NPs with UV-C irradiation reduced bacterial counts in pomegranate juice below the detection limit, but this method still needed a longer time. Furthermore, graphene-TiO₂ nanocomposites, despite being studied for wastewater treatment applications, exhibited a lower bacterial inactivation rate and required prolonged incubation to achieve their effects. Silver and gold-based nanomaterials demonstrated excellent antibacterial performance, but they also posed concerns regarding nanoparticle aggregation, cytotoxicity, and cost limitations. While silver nanoparticles are widely used in antibacterial coatings and water disinfection, the current nanochitosan-based system offers a more environmentally friendly alternative, avoiding metal ion toxicity concerns, while maintaining a rapid disinfection capability. Thus, the current approach presents a fast, effective, and possibly scalable nanomaterial-based disinfection method, demonstrating enhanced efficacy, shorter treatment duration, and improved safety, making it a promising solution for microbial control in water treatment applications.

3.5. SEM analysis of NPs

The surface morphology and structural properties of the NC and GO NPs were characterized by SEM before the UV LED

activation. The SEM analysis indicated that most of the NC particles were mostly spherical in shape, and moderately uniform in size distribution (Fig. 6A and B).^{59,60} The surface morphology indicated a slightly rough texture with a pronounced tendency for particles to aggregate, critical for understanding the available surface area for interaction with microbial cells during the bacterial inactivation process.^{61,62}

On the other hand, the SEM images of GO showed an irregular, flake-like morphological structure with some wrinkles and folds (Fig. 6C and D).⁶³ The layered nature of these sheets becomes critical in some of their functional interventions, including the generation of ROS under light activation. Wrinkles and folds present in GO sheets increase the active surface area.⁶⁴ They, hence, may enhance the capacity for light absorption and promote ROS generation under UV or visible light activation. Various studies have shown that GO efficiency in generating ROS correlates with its surface morphology; the layered structure is hence vital for its functional applications in disinfection and antibacterial activities.⁶⁴ Additionally, previous studies have shown that a good dispersion of GO in a matrix or solution enhances its performance, likely due to the uniform distribution of its functional groups.⁶⁵ Hence, the control of agglomeration becomes crucial in order to maximize the antibacterial activity in GO.

3.6. FTIR spectra of NPs with and without LED treatment

The FTIR spectra of GO/NC NPs without LED (Wo/T) and LED-treated GO/NC NPs (365 nm, 395 nm, and 455 nm) were analyzed to investigate the effect of UV treatment on the functional groups and chemical structure of these NPs. The spectra reveal characteristic peaks of oxygen-containing functional groups, including –OH, –COOH, –C–O–C, and alkoxy (–C–O), which are typical for GO (Fig. 7B).^{66,67} The LED-treated GO NP shows a typical –OH peak between 3600 and 3000 cm⁻¹, which is attributed to the O–H stretching vibrations, indicative of absorbed water molecules,⁶⁸ with



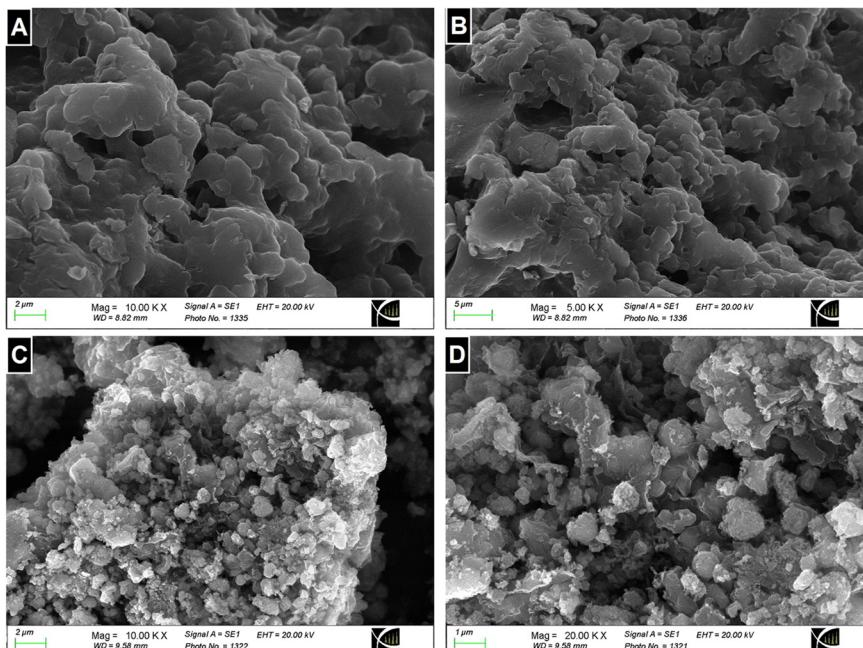


Fig. 6 SEM images of NC (A & B) and GO NPs (C & D).

intensity reductions after LED treatment suggesting partial removal of these groups without significant peak shifts, indicating retained hydrogen bonding (Fig. 7B).⁶⁹ A minor change was observed in the peak around 1723 cm^{-1} , which is attributed to the C=O stretching of carboxyl groups present at the edges of GO sheets (Fig. 7B).⁷⁰ A slight reduction in the peak intensity after the LED treatment points to a partial photoreduction of carboxyl groups due to UV exposure.⁷¹

The peak at approximately 1621 cm^{-1} , which corresponds to the stretching vibrations of aromatic C=C bonds in the sp^2 -hybridized carbon network of GO, remains consistent across all samples (Fig. 7B).⁷² This suggests that the structural integrity of GO's sp^2 -carbon network remains intact despite exposure to UV light at different wavelengths. The ($-\text{C}-\text{O}-\text{C}$) group stretching, represented by the peak around 1125 cm^{-1} , also shows a significant and uniform reduction in intensity across all treatments. This reduction suggests partial photoreduction of epoxy groups; such changes could enhance the antimicrobial properties of the GO water suspension, as the reduction of oxygen-containing groups increases the availability of active sites for microbial interaction.⁷³ Additionally, the reduction in epoxy groups might increase the electron-donating capacity of GO, promoting oxidative stress in microbial cells by generating ROS.³⁰ Additionally, the ($-\text{C}-\text{O}$) group stretching vibration, seen around 1000 cm^{-1} , shows a similar reduction in intensity.

The FTIR spectra of NC samples, both untreated and treated with UV light at wavelengths of 365 nm, 395 nm, and 455 nm, reveal that the peak positions remain stable across all samples, with no significant shifts observed, indicating that the fundamental chemical structure of NC remains intact post-treatment (Fig. 7A). A strong, broad

absorption band at approximately 3400 cm^{-1} , attributed to $-\text{OH}$ and $\text{N}-\text{H}$ stretching vibrations, is present in all samples.⁷⁴

Similarly, the peaks corresponding to the symmetric and asymmetric C-H stretching vibrations near 2850 cm^{-1} and 2930 cm^{-1} , characteristic of the methylene ($-\text{CH}_2-$) groups, exhibit no changes in position between the treated and untreated samples.⁷⁴ This indicates that the aliphatic chains in the NC structure are preserved during UV exposure. The carbonyl (C=O) stretching vibration at approximately 1640 cm^{-1} , which is a key feature of the amide groups in NC, shows no shift in peak position across the spectra (Fig. 7A). The stability of this peak indicates that the carbonyl functionalities, central to the NC structure, remain unaffected by UV treatment.³² Additionally, the C=O symmetric stretching and CH_2 bending around 1460 cm^{-1} show no shifts, further indicating the retention of these structural components after treatment (Fig. 7A).⁷⁵ The peaks corresponding to phosphate groups and ether linkages, observed at 1270 cm^{-1} , 1380 cm^{-1} , 1157 cm^{-1} , and 1070 cm^{-1} , also remain unchanged in position, suggesting that the P=O stretching and C-O-C linkages in the NC structure are stable under UV exposure.⁷⁶ The absence of any shifts in these regions confirms that the polysaccharide backbone and phosphate-related functionalities in NC are not altered by UV treatment.

3.7. Physicochemical characteristics of NP suspensions after LED treatments

The physicochemical properties of water samples containing NPs treated by LEDs were determined. The type of LED (wavelength of light radiation), NPs, and their interaction



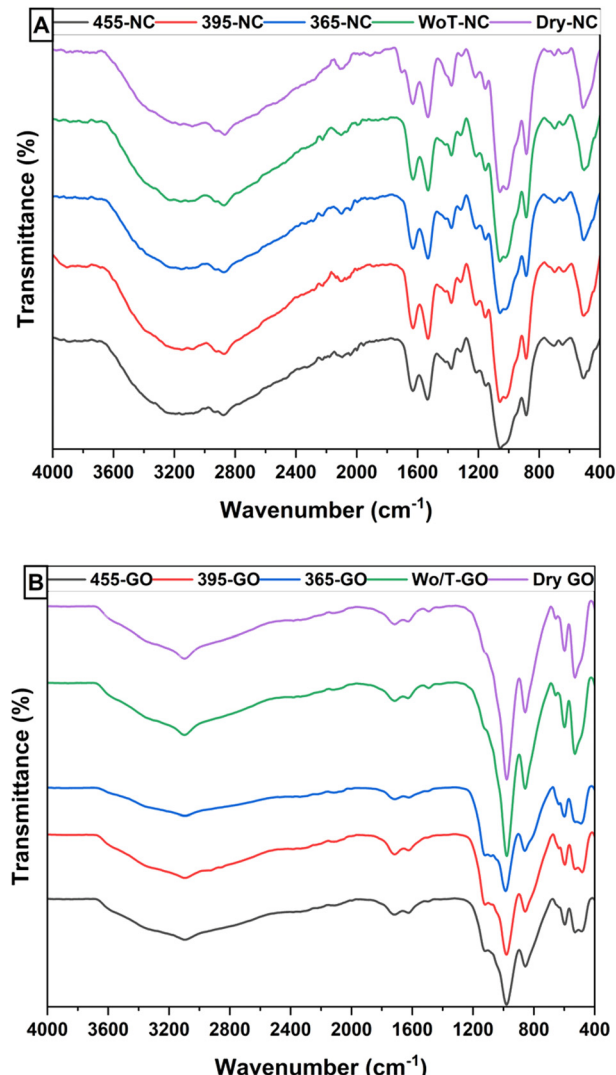


Fig. 7 FTIR spectra of (A) NC (control and LED treated samples) and (B) GO (control and LED treated samples). 365-NC/GO, 395-NC/GO, and 455-NC/GO represents NP samples (powder) extracted from 20 min LED and NP treated aqueous suspensions, dry-NC/GO represents untreated powder NPs, and WoT-NC/GO represents dried NPs extracted from 10 mL of aqueous suspension without LED treatment.

influenced these properties, including electrical conductivity, pH, and ORP.

The electrical conductivity of water samples with NPs alone, without the LED treatment, was significantly lower ($P < 0.05$). However, the water samples with GO exhibited a significantly ($P < 0.05$) higher electrical conductivity value than the water samples with NC at the same concentrations. Primarily, the dissolution of GO in an aqueous environment triggers the ionization of its various oxygen-containing functional groups, leading to the release of protons (H^+) and other ions into the GO suspension.⁷⁷ This combination makes the environment more acidic and electrically conductive, acting directly on bacterial cells by breaking down cellular membrane integrity or electrolyzing surface molecules on bacterial cells. The electrical conductivities of

GO suspensions in combination with 10- and 20 min LED treatment were almost similar. In line with these properties, all combinations of GO and LEDs at 365, 395, and 455 nm displayed an *E. coli* inactivation below the LOD. The individual GO-treated suspensions also had significantly higher ($P < 0.05$) electrical conductivity than NC suspensions. The LED-treated NC suspensions, as well as the individual NC suspensions, resulted in a significantly lower ($P < 0.05$) electrical conductivity than the individual GO or LED-treated GO suspensions (Fig. 8). This could be likely due to their structure and limited ability to release ions, which restricts their effectiveness in facilitating proton conduction.⁷⁸

The pH values of water samples containing NC and GO treated with LEDs were generally lower than the other water samples (Fig. 9). The most significant ($P < 0.05$) pH decrease was observed for water samples containing GO treated with LEDs, regardless of the wavelength of the LED. As mentioned earlier, the dissolution of GO in water initiates the ionization of its oxygen-containing functional groups, resulting in the release of protons (H^+). This contributes to the acidic nature of GO. Consequently, compared to GO suspensions, the pH values obtained with individual LED or NC treatments were much higher, indicating a less acidic environment. The higher pH of the NC suspension indicates its alkalinity, likely due to the amine groups in chitosan, which can accept protons and contribute to the basic nature of the solution. However, the pH values of LED-treated NC suspensions were significantly lower ($P < 0.05$) than those obtained after the LED treatment alone, which ranged from 5.72 to 5.95, or the pH value of the untreated water alone (pH = 6.81).

Water samples treated with LEDs alone showed a significant increase ($p < 0.05$) in the ORP value when compared to the control water sample (214 mV). This increase in the ORP was consistent at all three LED wavelengths (365 nm, 395 nm, and 455 nm). This indicates that LED irradiation enhances oxidative processes in the water. However, the level of enhancement in ORP depends on the LED wavelength used. For instance, water samples treated with the 365 nm LED showed significantly greater ($p < 0.05$) values than the 395 and 455 nm LEDs, as shown in Fig. 10. Based on our results, the ORP for all GO suspensions treated with different LEDs was significantly higher ($P < 0.05$). Higher ORP values enhance the production of ROS such as 1O_2 , which makes the suspension more reactive by facilitating electron transfer reactions and creating an oxidized environment, leading to a greater inactivation of *E. coli* inactivation achieved with combined GO and LED treatments.

The LED-treated NC suspensions displayed relatively lower ORP values than the LED-treated GO suspensions. Additionally, NC alone exhibited significantly lower ($P < 0.05$) ORP than GO (Fig. 10). This reflects a weaker oxidative capacity, consistent with its reduced efficacy in microbial inactivation. The collective effect of electrical conductivity,



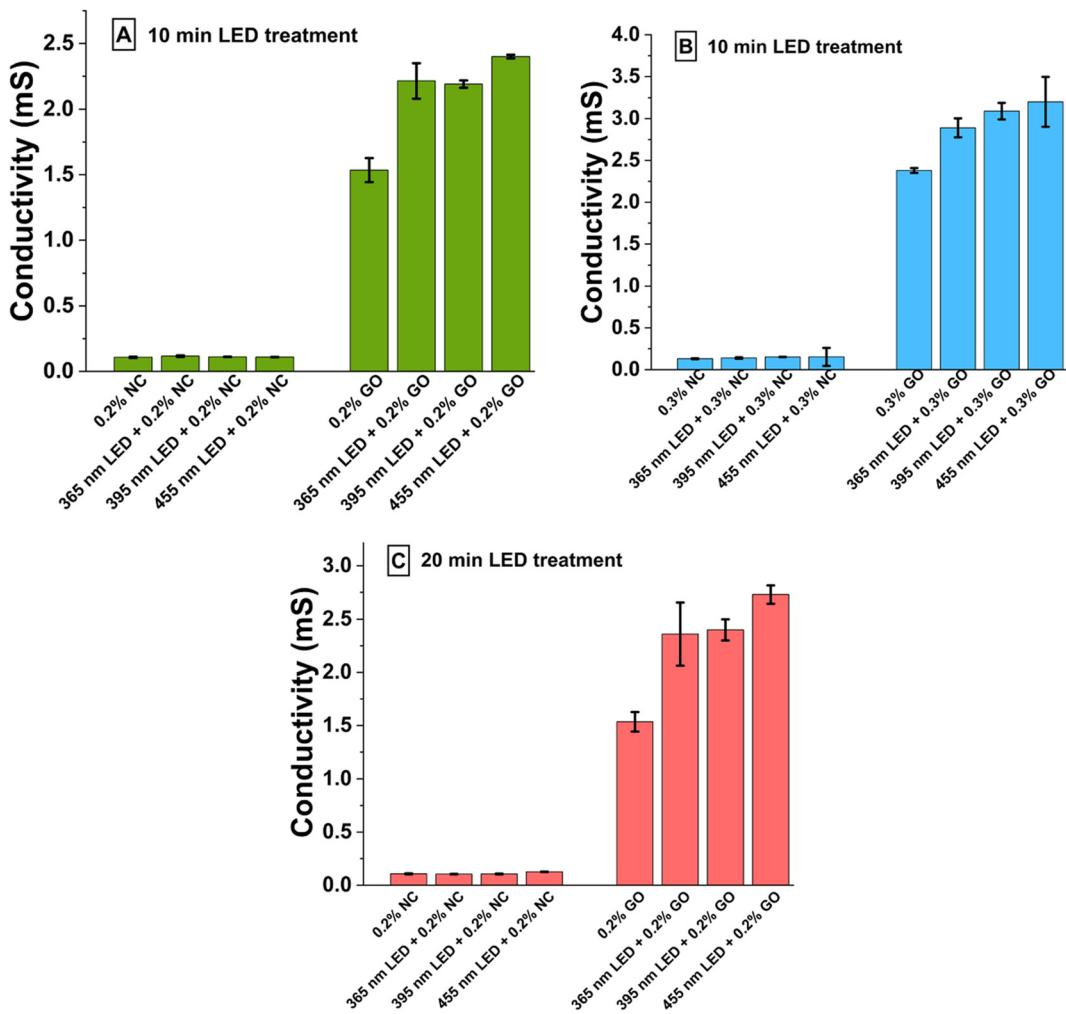


Fig. 8 Electrical conductivity values of water samples: (A) 0.2% NP with/without 10 min LED treatments, (B) 0.3% NP with or without 10 min LED treatments, and (C) 0.2% NP with/without 20 min LED treatments.

pH, and ORP in the combined NP and LED treated suspensions, particularly in GO and LED combinations, synergistically contributed to the greater inactivation of *E. coli*, with each factor playing a vital role in creating a highly reactive and hostile environment.

3.8. Physicochemical characteristics of NP + H₂O₂ suspensions after 365 nm LED treatment

The measured physicochemical properties of the water samples treated with the combinations of NPs, the 365 nm LED, and H₂O₂ showed a distinct relationship with their respective microbial inactivation efficiencies. The combined GO + 365 nm LED and H₂O₂ treatments showed more favourable physicochemical properties, which are more effective for microbial inactivation than NC + 365 nm LED and H₂O₂ samples (Table 2). Despite this, the GO + 365 nm LED and H₂O₂ combination displayed a significantly lower ($P < 0.05$) *E. coli* inactivation effectiveness. This could be partly related to the radical scavenging properties of graphene-based materials,⁵¹ *i.e.*, GO is considered an effective

scavenger of 'OH radicals.⁵¹ Such radical-scavenging properties could reduce the amount of high 'OH available for the inactivation of *E. coli* during the treatment.⁵¹ Nevertheless, the reduction in the *E. coli* population achieved with GO + 365 nm LED and H₂O₂ could be partially linked to these physiochemical values, such as higher ORP and electrical conductivity along with a lower pH.

In contrast, it was reported that H₂O₂, when combined with NC, degrades NC.⁷⁹ This leads to a decrease in the molecular weight of NC along with its viscosity leading to a better penetration of NC into the *E. coli* cell membrane. In contrast, the decreased viscosity would allow it to flow easily, leading to a better distribution and interaction with the *E. coli* surface. Additionally, H₂O₂ has been found to oxidize the -OH and -NH₂ groups of NC, yielding -COOH groups, making it highly reactive against *E. coli*.⁷⁹ Apart from this, the significant level of ORP and pH contributed to the overall effectiveness of the combined NC + 365 nm LED + H₂O₂ treatment.

Although the combined treatment of the 365 nm LED and H₂O₂ had a relatively higher ORP value, an apparent



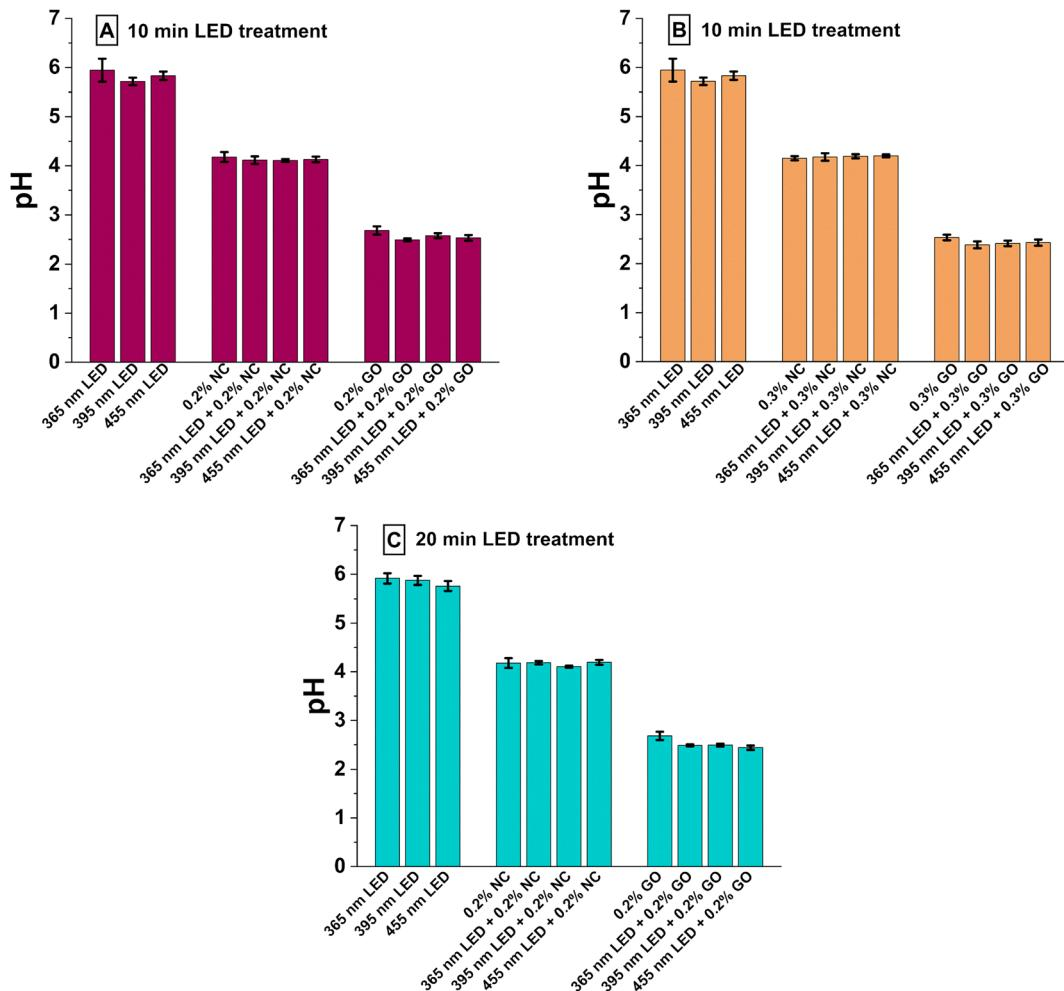


Fig. 9 pH values of water samples: (A) 0.2% NP with/without 10 min LED treatment, (B) 0.3% NP with/without 10 min LED, and (C) 0.2% NP with/without 20 min LED.

LED treatment time- and H_2O_2 concentration-dependent pattern was observed in *E. coli* inactivation (Fig. 5), (Table 2). This highlights that the inactivation was not solely driven by the changes in ORP or pH but was more closely linked to the synergistic effect between H_2O_2 and UV light, which could increase the 'OH production.^{26,80} The individual treatments, such as NPs, the 365 nm LED or H_2O_2 , displayed a greater ORP, electrical conductivity, and a lower pH, particularly in the case of GO samples (ESI† Table S2). The shorter treatment time of 1 and 3 min could be a contributing factor leading to a lower *E. coli* reduction achieved with these individual treatments. Additionally, these individual treatments failed to achieve a significant effect on *E. coli* inactivation, underscoring the potential limitations of using each treatment individually.

4. Conclusions

The antibacterial efficacy of 365, 395, and 455 nm LEDs against *E. coli* AW1.7 in water was investigated, with the

365 nm LED showing a promising antibacterial effect against *E. coli*. GO and NC displayed *E. coli* inactivation in water at different concentrations. Between these two, GO was found to be the most effective NP against *E. coli*. The unique physiochemical properties of GO enable them to interact with bacterial cells, leading to higher cell death. The antimicrobial effectiveness of light pulses emitted from different LEDs (365, 395, and 455 nm) in combination with NC and GO demonstrated significant *E. coli* inactivation in water. The GO suspension resulted in *E. coli* inactivation mostly below the LOD, regardless of the LED used. In contrast, the NC suspension showed greater *E. coli* inactivation with the 365 nm LED, followed by the 395 nm LED. The effect of UV LED treatment time was evident in the case of NC. The incorporation of H_2O_2 and 365 nm LED treatment indicated that higher H_2O_2 concentration, combined with a shorter LED treatment time, resulted in *E. coli* inactivation below the LOD. Additionally, the effect of a lower concentration of H_2O_2 was found to be partially compensated by increasing the 365 nm LED treatment time. The addition of NC and GO NPs to H_2O_2 prior to the 365



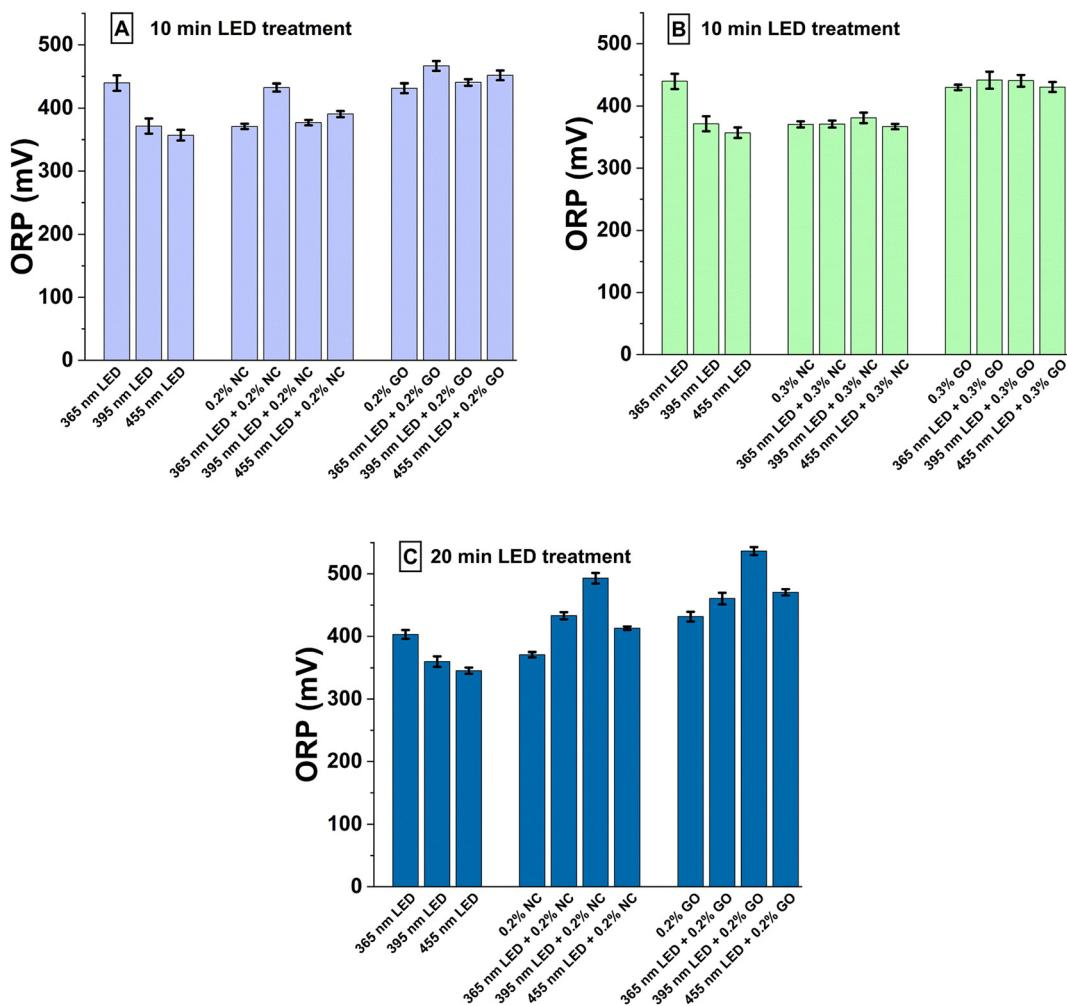


Fig. 10 ORP values of water samples: (A) 0.2% NP with/without 10 min LED treatment, (B) 0.3% NP with/without 10 min LED, and (C) 0.2% NP with/without 20 min LED treatment.

Table 2 Effect of selected concentration of NP, H_2O_2 , and 365 nm LED treatments in different combinations

H_2O_2 concentration (M)	NP concentration (0.2%; unless specified)	365 nm LED treatment time (min)	ORP (mV)	Electrical conductivity (mS)	pH
0.1	NC	1	417.5 ± 17.7^a	0.16 ± 0.1^a	4.1 ± 0.1^a
	GO	1	499.0 ± 2.80^b	1.45 ± 0.1^b	2.5 ± 0.0^b
0.01	NC	1	402.0 ± 2.80^a	0.11 ± 0.0^a	4.1 ± 0.1^a
	GO	1	490.5 ± 4.90^b	1.12 ± 0.0^b	2.6 ± 0.1^b
0.01	NC	3	411.0 ± 4.20^a	0.16 ± 0.0^a	4.2 ± 0.0^a
	GO	3	490.0 ± 2.80^b	1.31 ± 0.2^b	2.7 ± 0.1^b
0	NC	1	399.0 ± 8.50^a	0.14 ± 0.0^a	4.1 ± 0.0^a
	GO	1	472.0 ± 9.90^b	1.84 ± 0.1^b	2.4 ± 0.0^b
0	NC	3	401.0 ± 4.20^a	0.15 ± 0.0^a	4.1 ± 0.1^a
	GO	3	505.0 ± 9.90^b	1.19 ± 0.0^b	2.5 ± 0.1^b
0.1	0	1	352.5 ± 6.40^a	0.00 ± 0.0^a	5.1 ± 0.1^b
0.01	0	1	350.0 ± 2.80^a	0.00 ± 0.0^a	4.1 ± 0.1^a
0.01	0	3	364.0 ± 11.30^a	0.00 ± 0.0^a	5.2 ± 0.1^b
0.1	NC	0	407.0 ± 4.90^a	0.17 ± 0.1^a	4.1 ± 0.0^a
	GO	0	497.5 ± 7.80^b	1.60 ± 0.3^b	2.6 ± 0.2^b
0.01	NC	0	407.0 ± 5.70^a	0.16 ± 0.0^a	4.1 ± 0.1^a
	GO	0	497.5 ± 4.90^b	1.25 ± 0.1^b	2.6 ± 0.1^b

For example, for the measurement of ORP, the subscripts show significant difference between the treatments NC and GO with H_2O_2 concentration of 0.1% and 365 nm LED treatment for 1 min (first and second row of the Table).

nm LED treatment resulted in higher *E. coli* inactivation, particularly with the LED + NC + H₂O₂ combination, and this mainly relied on the LED treatment time and H₂O₂ concentration used.

Data availability

Data are available on request.

Author contributions

Rahul Chetry: conceptualization, methodology, investigation, writing – original draft, review & editing. Adityasukumar Pasagadi: methodology, investigation, review & editing. Muhammad Zubair: methodology, review & editing. Aman Ullah: conceptualization, funding acquisition, methodology, resources, supervision, writing – review & editing. M. S. Roopesh: conceptualization, funding acquisition, methodology, resources, supervision, writing – review & editing.

Conflicts of interest

There are no conflicts of interest to declare in this work.

Acknowledgements

The authors would like to thank the Results Driven Agriculture Research (RDAR) and the Canadian Agricultural Partnership (CAP) for their financial support.

References

- 1 UN-Water, UN-Water integrated monitoring initiative, *UN-Water website*, 2021, 1–58, <https://www.unwater.org/our-work/integrated-monitoring-initiative-sdg-6>.
- 2 P. G. Pierpaoli, *United Nations Educational Scientific and Cultural Organization*, 2010, vol. 44, pp. 1293–1294.
- 3 S. Sharma, P. Sachdeva and J. S. Virdi, *Appl. Microbiol. Biotechnol.*, 2003, **61**, 424–428.
- 4 A. Ojha, *Nanomaterials for removal of waterborne pathogens*, Elsevier, 2020.
- 5 N. N. Shulga and I. S. Shulga, *Eurasian Union of Scientists*, 2020, **1**, 31–33.
- 6 A. A. Lanrewaju, A. M. Enitan-Folami, S. Sabiu and F. M. Swalah, *Front. Microbiol.*, 2022, **13**, 991856.
- 7 W. N. Lee, C. H. Huang and G. Zhu, *Food Chem.*, 2018, **256**, 319–326.
- 8 S. D. Richardson, M. J. Plewa, E. D. Wagner, R. Schoeny and D. M. DeMarini, *Mutat. Res., Rev. Mutat. Res.*, 2007, **636**, 178–242.
- 9 Q. Li, S. Mahendra, D. Y. Lyon, L. Brunet, M. V. Liga, D. Li and P. J. J. Alvarez, *Water Res.*, 2008, **42**, 4591–4602.
- 10 A. Kassem, G. M. Ayoub and L. Malaeb, *Sci. Total Environ.*, 2019, **668**, 566–576.
- 11 S. Y. Rikta, *Application of Nanoparticles for Disinfection and Microbial Control of Water and Wastewater*, Elsevier Inc., 2019.
- 12 D. K. Kim and D. H. Kang, *Appl. Environ. Microbiol.*, 2018, **84**, e00944–18.
- 13 M. Kneissl, T. Y. Seong, J. Han and H. Amano, *Nat. Photonics*, 2019, **13**, 233–244.
- 14 K. Song, M. Mohseni and F. Taghipour, *Water Res.*, 2016, **94**, 341–349.
- 15 X. Luo, B. Zhang, Y. Lu, Y. Mei and L. Shen, *J. Hazard. Mater.*, 2022, **421**, 126682.
- 16 S. L. Gora, K. D. Rauch, C. C. Ontiveros, A. K. Stoddart and G. A. Gagnon, *Water Res.*, 2019, **151**, 193–202.
- 17 X. Y. Zou, Y. L. Lin, B. Xu, T. C. Cao, Y. L. Tang, Y. Pan, Z. C. Gao and N. Y. Gao, *Sci. Total Environ.*, 2019, **650**, 210–215.
- 18 N. Elmnasser, S. Guillou, F. Leroi, N. Orange, A. Bakhrouf and M. Federighi, *Can. J. Microbiol.*, 2007, **53**, 813–821.
- 19 A. Prasad, M. Gänzle and M. S. Roopesh, *Appl. Sci.*, 2023, **13**, 1501.
- 20 L. Zhang, D. Pornpattananangkul, C.-M. Hu and C.-M. Huang, *Curr. Med. Chem.*, 2010, **17**, 585–594.
- 21 A. Raghunath and E. Perumal, *Int. J. Antimicrob. Agents*, 2017, **49**, 137–152.
- 22 V. Palmieri and M. Papi, *Nano Today*, 2020, **33**, 100883.
- 23 I. Aranaz, M. Mengibar, R. Harris, I. Panos, B. Miralles, N. Acosta, G. Galed and A. Heras, *Curr. Chem. Biol.*, 2009, **3**, 203–230.
- 24 S. Liu, T. H. Zeng, M. Hofmann, E. Burcombe, J. Wei, R. Jiang, J. Kong and Y. Chen, *ACS Nano*, 2011, 1–11.
- 25 C. B. Chidambara Raj and L. H. Quen, *Chem. Eng. Sci.*, 2005, **60**, 5305–5311.
- 26 M. Oturan and J.-J. Aaron, *Crit. Rev. Environ. Sci. Technol.*, 2014, **44**, 2577–2641.
- 27 V. Ghate, A. Kumar, M. J. Kim, W. S. Bang, W. Zhou and H. G. Yuk, *J. Food Eng.*, 2017, **196**, 130–138.
- 28 Y. Zhang, S. F. Ali, E. Dervishi, Y. Xu, Z. Li, D. Casciano and A. S. Biris, *J. Am. Chem. Soc.*, 2010, **4**, 3181–3186.
- 29 Y. Chong, C. Ge, G. Fang, R. Wu, H. Zhang, Z. Chai, C. Chen and J. J. Yin, *Environ. Sci. Technol.*, 2017, **51**, 10154–10161.
- 30 S. Liu, T. H. Zeng, M. Hofmann, E. Burcombe, J. Wei, R. Jiang, J. Kong and Y. Chen, *ACS Nano*, 2011, **5**, 6971–6980.
- 31 A. Pompella, A. Visvikis, A. Paolicchi, V. De Tata and A. F. Casini, *Biochem. Pharmacol.*, 2003, **66**, 1499–1503.
- 32 L. Qi, Z. Xu, X. Jiang, C. Hu and X. Zou, *Carbohydr. Res.*, 2004, **339**, 2693–2700.
- 33 R. C. Goy, D. De Britto and O. B. G. Assis, *Polimeros*, 2009, **19**, 241–247.
- 34 A. Hamamoto, M. Mori, A. Takahashi, M. Nakano, N. Wakikawa, M. Akutagawa, T. Ikehara, Y. Nakaya and Y. Kinouchi, *J. Appl. Microbiol.*, 2007, **103**, 2291–2298.
- 35 G. F. Kramer and B. N. Ames, *J. Bacteriol.*, 1987, **169**, 2259–2266.
- 36 S. Kozmin, G. Slezak, A. Reynaud-Angelin, C. Elie, Y. De Rycke, S. Boiteux and E. Sage, *Proc. Natl. Acad. Sci. U. S. A.*, 2005, **102**, 13538–13543.
- 37 S. V. Gudkov, O. E. Karp, S. A. Garmash, V. E. Ivanov, A. V. Chernikov, A. A. Manokhin, M. E. Astashev, L. S. Yaguzhinsky and V. I. Bruskov, *Biophysics*, 2012, **57**, 1–8.
- 38 P. R. Gogate and A. B. Pandit, *Adv. Environ. Res.*, 2004, **8**, 501–551.



39 M. Mori, A. Hamamoto, A. Takahashi, M. Nakano, N. Wakikawa, S. Tachibana, T. Ikehara, Y. Nakaya, M. Akutagawa and Y. Kinouchi, *Med. Biol. Eng. Comput.*, 2007, **45**, 1237–1241.

40 M. J. Kim and H. G. Yuk, *Appl. Environ. Microbiol.*, 2017, **83**, e02582-16.

41 M. J. Kim, M. Mikš-Krajnik, A. Kumar and H. G. Yuk, *Food Control*, 2016, **59**, 99–107.

42 K. P. Loh, Q. Bao, G. Eda and M. Chhowalla, *Nat. Chem.*, 2010, **2**, 1015–1024.

43 M. Veerapandian, L. Zhang, K. Krishnamoorthy and K. Yun, *Nanotechnology*, 2013, **24**, 395706.

44 Y. H. Ding, P. Zhang, Q. Zhuo, H. M. Ren, Z. M. Yang and Y. Jiang, *Nanotechnology*, 2011, **22**(21), DOI: [10.1088/0957-4484/22/21/215601](https://doi.org/10.1088/0957-4484/22/21/215601).

45 X. H. Tai, S. W. Chook, C. W. Lai, K. M. Lee, T. C. K. Yang, S. Chong and J. C. Juan, *RSC Adv.*, 2019, **9**, 18076–18086.

46 L. Vannozzi, E. Catalano, M. Telkhozhayeva, E. Teblum, A. Yarmolenko, E. S. Avraham, R. Konar, G. D. Nessim and L. Ricotti, *Nanomaterials*, 2021, **11**, 2105.

47 K.-H. Liao, Y.-S. Lin, C. W. Macosko and C. L. Haynes, *ACS Appl. Mater. Interfaces*, 2011, **3**, 2607–2615.

48 T. Du, A. S. Adeleye, T. Zhang, C. Jiang, M. Zhang, H. Wang, Y. Li, A. A. Keller and W. Chen, *Environ. Sci.: Nano*, 2018, **5**, 2590–2603.

49 Y. Nitzan, M. Salmon-Divon, E. Shporen and Z. Malik, *Photochem. Photobiol. Sci.*, 2004, **3**, 430–435.

50 F. Shahidi, J. K. V. Arachchi and Y. J. Jeon, *Trends Food Sci. Technol.*, 1999, **10**, 37–51.

51 Y. Qiu, Z. Wang, A. C. E. Owens, I. Kulaots, Y. Chen, A. B. Kane and R. H. Hurt, *Nanoscale*, 2014, **6**, 11744–11755.

52 A. Rubio-Clemente, E. Chica and G. Peñuela, *Environ. Sci. Pollut. Res.*, 2019, **26**, 4462–4473.

53 J. A. Imlay, *Annu. Rev. Biochem.*, 2008, **77**, 755–776.

54 V. Denisova, L. Mezule and T. Juhna, *Water Pract. Technol.*, 2022, **17**, 537–543.

55 E. Araby, H. H. Abd El-Khalek and M. S. Amer, *J. Food Process. Preserv.*, 2022, **46**, 1–15.

56 R. Darini, H. Ahari, A. Khosrojerdi, B. Jannat and H. Babazadeh, *Sci. Rep.*, 2025, **15**, 1–12.

57 W. R. Li, X. B. Xie, Q. S. Shi, H. Y. Zeng, Y. S. Ou-Yang and Y. Ben Chen, *Appl. Microbiol. Biotechnol.*, 2010, **85**, 1115–1122.

58 Y. Zhou, Y. Kong, S. Kundu, J. D. Cirillo and H. Liang, *J. Nanobiotechnol.*, 2012, **10**, 1–9.

59 W. Yang, J. Fu, T. Wang and N. He, *J. Biomed. Nanotechnol.*, 2009, **5**, 591–595.

60 M. Agarwal, M. K. Agarwal, N. Shrivastav, S. Pandey, R. Das and P. Gaur, *Int. J. Life Sci. Sci. Res.*, 2018, **4**, 1713–1720.

61 Z. Q. Su, H. L. Zhang, S. H. Wu, Y. Tao and L. Q. Zang, *J. Nanomater.*, 2010, **2010**, 898910.

62 Y. Luo, *J. Food Process. Beverages*, 2013, **1**, 13.

63 S. Deng and V. Berry, *Mater. Today*, 2016, **19**, 197–212.

64 J. Wang, B. Chen and B. Xing, *Environ. Sci. Technol.*, 2016, **50**, 3798–3808.

65 S. J. Lee, S. J. Yoon and I.-Y. Jeon, *Polym.*, 2022, **14**, 4733.

66 H. Korucu, A. I. Mohamed, A. Yartaşı and M. Uğur, *Chem. Pap.*, 2023, **77**, 5787–5806.

67 P. Wu, P. Du, H. Zhang and C. Cai, *Phys. Chem. Chem. Phys.*, 2013, **15**, 6920–6928.

68 C. H. Manoratne, S. R. D. Rosa and I. R. M. Kotegoda, *Mater. Sci. Res. India*, 2017, **14**, 19–30.

69 X. Yuan, D. Peng, Q. Jing, J. Niu, X. Cheng, Z. Feng and X. Wu, *Nanomaterials*, 2018, **8**, 654.

70 F. Amato, A. Motta, L. Giaccari, R. Di Pasquale, F. A. Scaramuzzo, R. Zanoni and A. G. Marrani, *Nanoscale Adv.*, 2023, **5**, 893–906.

71 B. Xue, Y. Zou and Y. Yang, *J. Mater. Sci.*, 2017, **52**, 4866–4877.

72 S. Kumuda, U. Gandhi, U. Mangalanathan and K. Rajanna, *J. Mater. Sci.: Mater. Electron.*, 2024, **35**, 637.

73 F. Perreault, A. F. De Faria and M. Elimelech, *Chem. Soc. Rev.*, 2015, **44**, 5861–5896.

74 J. J. Joseph, D. Sangeetha and T. Gomathi, *Int. J. Biol. Macromol.*, 2016, **82**, 952–958.

75 L. Wang and A. Wang, *J. Hazard. Mater.*, 2007, **147**, 979–985.

76 N. Maganti, P. K. C. Venkat Surya, W. W. Thein-Han, T. C. Pesacreta and R. D. K. Misra, *Adv. Eng. Mater.*, 2011, **13**, 108–122.

77 W. Du, H. Wu, H. Chen, G. Xu and C. Li, *Carbon*, 2020, **158**, 568–579.

78 S. N. Asnin, Wahab, D. Permana, L. O. Ahmad, S. H. Sabarwati and L. O. A. Ramadhan, *WSEAS Trans. Power Syst.*, 2016, **11**, 183–189.

79 K. S. Huang, Y. R. Sheu and I. C. Chao, *Polym.-Plast. Technol. Eng.*, 2009, **48**, 1239–1243.

80 E. J. Rosenfeldt, K. G. Linden, S. Canonica and U. von Gunten, *Water Res.*, 2006, **40**, 3695–3704.

